

Terahertz Modulation of Hexagonal-Shaped Metamaterials Employing ZnO Quantum Dots

Clarissa D. Vázquez-Colón¹, Alvaro Flores-Pacheco², Janeth Alexandra García-Monge¹,
Juan Adrián Zepeda-Galvéz¹, Daniel Shreiber³, Arturo Ayón^{1*}

¹The University of Texas at San Antonio, San Antonio, Texas, USA

²Departamento de Física, Universidad de Sonora, Hermosillo, Sonora, México

³US Army Research Laboratory, Aberdeen Proving Ground, MD, USA

Email: *aayon@utsa.edu

How to cite this paper: Vázquez-Colón, C.D., Flores-Pacheco, A., García-Monge, J.A., Zepeda-Galvéz, J.A., Shreiber, D. and Ayón, A. (2019) Terahertz Modulation of Hexagonal-Shaped Metamaterials Employing ZnO Quantum Dots. *Open Journal of Inorganic Non-metallic Materials*, 9, 1-13. <https://doi.org/10.4236/ojinm.2019.91001>

Received: January 2, 2019

Accepted: January 28, 2019

Published: January 31, 2019

Copyright © 2019 by author(s) and Scientific Research Publishing Inc. This work is licensed under the Creative Commons Attribution International License (CC BY 4.0).

<http://creativecommons.org/licenses/by/4.0/>



Open Access

Abstract

The utilization of UV excitation to verify the terahertz (THz) wave modulation of hexagonal-shaped metamaterial (MM) arrays coated with synthesized photoluminescent, down-shifting ZnO quantum dots (QDs) of two different radius sizes, namely, 3.00 nm (pH 10) and 2.12 nm (pH 12), respectively is reported. In order to characterize the behavior of the MM before and after deployment of the ZnO QDs, THz time domain spectroscopy in transmission mode was employed. Upon exposure to UV excitation, the collected amplitude modulation values were 9.21% for the pH 12 and 4.55% for the pH 10 ZnO QDs, respectively. It is anticipated that the ability to actively tune the performance of otherwise passive structures will promote the proliferation of THz signal modulation devices in the near future.

Keywords

Terahertz, Metamaterials, Quantum Dots, Terahertz Spectroscopy, Modulation

1. Introduction

The terahertz (THz) portion of the electromagnetic spectrum is located between the microwave and infrared segments and has remained relatively underdeveloped because the power output of conventional electronic circuitry (*i.e.*, IMPATT, MMIC, Gunn, TUNNET, multiplexers, photomixers, RTD, etc.) drops significantly as the transition is made from the microwaves to the THz region. Similarly, photonic structures (*i.e.*, III-V lasers, QCL, etc.) also exhibit a similar and noticeable deterioration in the power output as the transition is made from

infrared to THz frequencies. In view of the unrelenting saturation of the electromagnetic spectrum, there is an increased interest in developing passive and active devices with suitable performance in the THz portion of the spectrum, including tunable structures that could alleviate said saturation. Additionally, THz electromagnetic waves are nonionizing and, for the same reason, attractive for applications where microwave interactions with organic materials could be a source of concern [1]-[10]. One option to overcome the performance limitations of conventional electronic circuitry and/or photonic devices at THz frequencies is the utilization of metamaterials (MMs), which are subwavelength, unit-cell laboratory-made structures that are fabricated to exhibit specific electromagnetic properties not encountered in naturally available materials. The topology encountered in MMs customarily consists of a metallic or polymeric array, in which the passive electromagnetic properties are determined by the dimensions of the unit cell, the fill factor of said cells and the materials employed in their fabrication [11]. Incorporating functional materials to MM designs capable of responding in real time to an external stimulus would improve tunability and, more generally, enable the demonstration of THz modulation devices [12] by modifying signal intensity, phase, propagation direction, beam shape or resonant frequency. To this end, the utilization of UV excitation with a wavelength of 400 nm, to verify the modulation of THz waves of a metamaterial array coated with previously synthesized photoluminescent, down-shifting ZnO QDs synthesized in colloidal solutions with pH values of 10 and 12, respectively, is discussed in this work.

2. Experimental Details

The employed MM array (see **Figure 1**) which has been described elsewhere [13], was fabricated using a conventional lift-off process on high resistivity, <100> silicon wafers and had dimensions such that the array exhibited a resonance frequency of 1 THz. The metallization of the tested MM structures was performed by evaporating 200 nm of silver on a 20 nm layer of chromium that served as an adhesion layer.

2.1. ZnO QD Synthesis

Colloidal ZnO QDs were synthesized at room temperature by a sonochemical

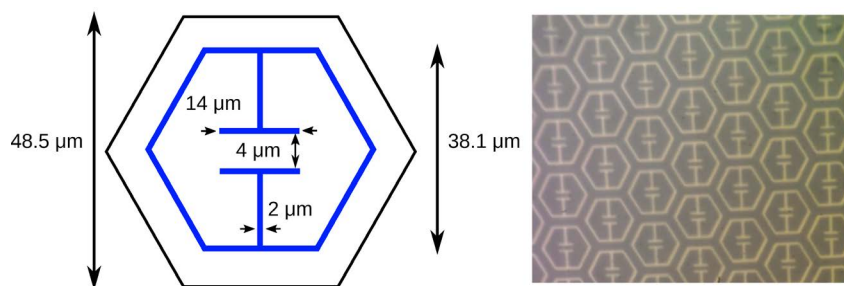


Figure 1. (a) Dimensions of the MM unit cell employed in this exercise. The black and blue lines represent the unit cell and metallic features, respectively. (b) Optical microscope image of the microfabricated array.

method [14] [15] in which acoustic cavitation precludes the formation of intermediate products, including $\text{Zn}(\text{OH})_2$, converts the reactants into ZnO QDs and calcination steps are not required. This method has proven useful for accelerating chemical reactions in liquid-solid systems [14]. Specifically, ZnO QD synthesis was accomplished by preparing an initial solution of 0.02 M zinc acetate (ZnAc) (99.99%, Sigma-Aldrich) in pure ethanol. A second and independent solution of 0.01 M of lithium hydroxide (LiOH) ($\geq 98\%$ Sigma-Aldrich) was prepared also in pure ethanol. Subsequently, the LiOH solution was incorporated dropwise to the ZnAc solution until a pH value of 10 or 12 was obtained. Once the targeted pH value was reached, the mixture was placed in a sonication bath for 3 hours [16] [17]. The chosen pH values were found to yield stable nanoparticles and relatively minimal agglomeration. Furthermore, the ultimate size of the obtained QDs was determined by the pH value of the final solution employed during synthesis and observed to be in agreement with the dependence of ZnO nanoparticle size on pH reported elsewhere [18]. A summary of the synthesis is shown in **Figure 2**. The ZnO QDs were then deposited onto the surface of the MM shown in **Figure 1**.

In order to characterize the synthesized ZnO QDs in the terahertz regime, the nanoparticles were dispersed in a polydimethylsiloxane (PDMS) matrix. To this end, the ZnO QDs were harvested by drying the final solution on a hotplate maintained at 70°C , and prior to dispersing them in the aforementioned matrix, the QD samples were thoroughly pulverized using a mortar. Once the solvent had completely evaporated, the ZnO QD powder was mixed with a PDMS solution that had been previously prepared by mixing 5 wt% of a curing agent in a silicone elastomer [19] [20]. The mixture of PDMS and ZnO QDs was then cured at 90°C for 3 hours (see **Figure 3**).

2.2. ZnO QD Absorption and Emission Characterization

The UV-vis absorption characterization of the ZnO QDs was performed using

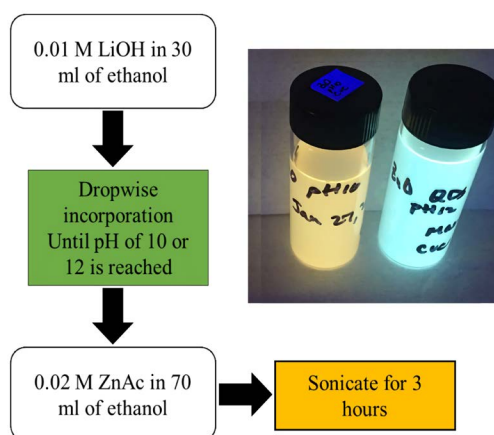


Figure 2. ZnO QD synthesis approach and their visual appearance under UV excitation. The synthesis pH values employed were 10 (yellowish solution on the left) and 12 (blue solution on the right).

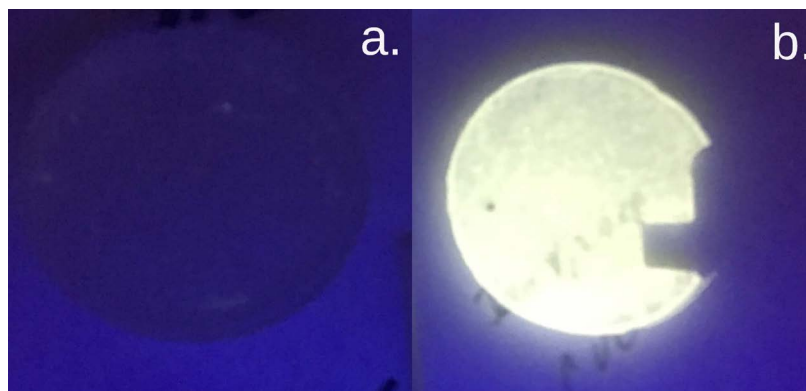


Figure 3. (a) Cured PDMS membranes exhibit no photoluminescent properties under UV excitation. (b) Observed photoluminescence of ZnO QDs synthesized with a pH value of 12 and dispersed in a PDMS matrix.

an Ocean Optics Flame-S-UV-VIS spectrometer and the collected absorption spectra corresponding to nanocrystals synthesized with the previously mentioned colloidal solution pH values of 10 and 12, are shown in **Figure 4**, along with their corresponding photoluminescent response. The emission wavelength is directly related to quantum dot size, therefore, the larger the nanoparticles the longer the wavelength of their characteristic photoluminescent peak [21] [22]. Thus, QDs synthesized with a pH value of 12 have an emission peak located at 510 nm, while QDs synthesized with a pH value of 10 have the peak located at 540 nm, indicating that lower pH values produce larger nanoparticles.

The observed QD absorbance measurements are related to QD bandgap by the following expression

$$\alpha = \left(\frac{A}{h\nu} \right) (h\nu - E_g)^m \quad (1)$$

where α is the absorption coefficient, A is an optical constant, m represents the type of optical transition in the semiconducting material; specifically, m can only take the values of 1/2, 2, 3/2 or 3 corresponding to allowed direct, allowed indirect, forbidden direct and forbidden indirect, respectively [23], and E_g is the band gap of the semiconducting quantum dots. Multiplying Equation (1) by $h\nu$, obtaining the natural logarithm and finally taking the derivative with respect to $h\nu$, the resultant equation is

$$\frac{d(\ln(\alpha h\nu))}{d(h\nu)} = \frac{m}{h\nu - E_g} \quad (2)$$

The bandgap can then be estimated by plotting Equation (2) with respect to energy [23], and this approach permits the identification of the inflection point (*i.e.*, the bandgap value) where the slope changes sign (see **Figure 5**). In other words, the bandgap value will be determined as a discontinuity at $h\nu - E_g = 0$ [23]. The extracted bandgap values were 3.43 eV and 3.62 eV for the ZnO QDs synthesized with the colloidal solutions with a pH of 10 and 12, respectively. The observed emission peaks were located at 510 nm (pH 12) and 540 nm (pH 10).

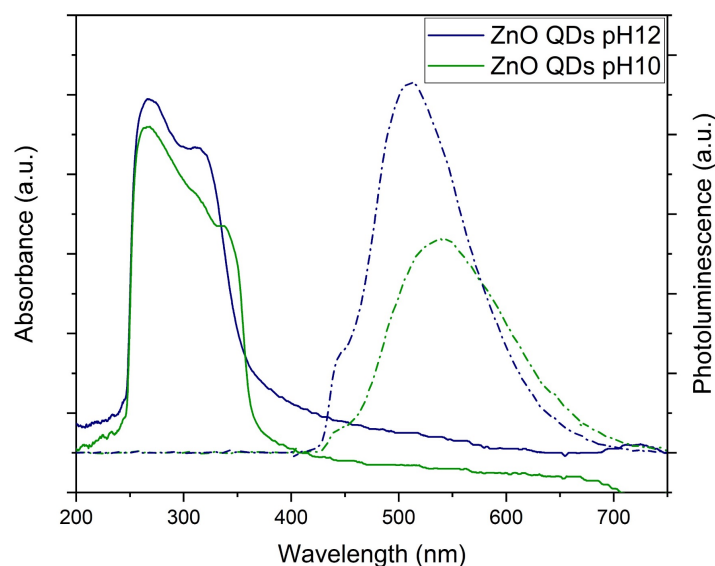


Figure 4. Collected absorbance spectra of the ZnO QDs colloidal solutions synthesized with pH values of 10 and 12 (solid lines), respectively. The dotted lines show the photoluminescence spectra of the corresponding ZnO quantum dot colloidal solutions.

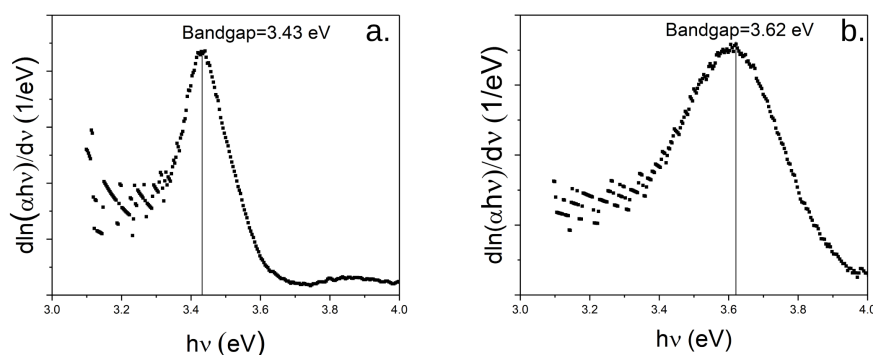


Figure 5. Estimated bandgap values of the ZnO QDs synthesized with pH values of 10 and 12, respectively.

Since the wavelength emission is directly related to QD size, *i.e.*, the larger the particle, the longer the wavelength of emission, the emission peak wavelength observations corroborate that higher pH values during synthesis indeed lead to smaller ZnO quantum dots.

Once the bandgap value had been calculated, the size of the QDs was estimated employing Brus' quantum mechanical approximation [24]

$$E_g = E_{Bulk} + \frac{\hbar^2 \pi^2}{2r^2} \left(\frac{1}{m_e^*} + \frac{1}{m_h^*} \right) - \frac{1.8e^2}{r\epsilon} \quad (3)$$

where E_g is the band gap energy of the semiconductor quantum dots, E_{Bulk} is the band gap energy of the bulk semiconductor material, \hbar is the reduced Planck constant, m_e^* and m_h^* represent the effective mass of electron and hole of the material under consideration, ϵ is the bulk relative permittivity, and r is the QD radius. For the pH 10 ZnO QDs we estimated a radius of 3.00 nm and

for the pH 12 ZnO QDs we obtained a radius of 2.12 nm. To corroborate the estimated sizes, transmission electron microscope (TEM) images for both samples were obtained and are shown in **Figure 6**. The measured values were approximately 3.2 nm and 1.85 nm radius for the ZnO pH 10 and ZnO pH 12 samples, respectively, in reasonable agreement with the sizes estimated via Equation (3).

3. Experimental Results and Discussion

The THz time domain spectroscopy (THz-TDS) characterization was performed by employing a Menlo Systems TeraSmart equipment [25], operated in transmission mode (see **Figure 7**). This system employs a photoconductive antenna based on an InGaAs/InAlAs multilayered mesa as the emitter and detector, which are activated by a femtosecond laser of wavelength 800 nm. The system

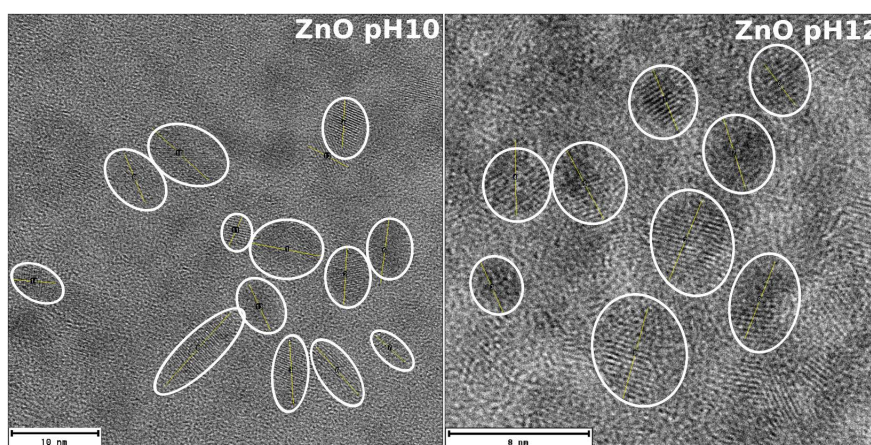


Figure 6. ZnO pH10 and ZnO pH12 TEM images used to corroborate sizes estimated values.

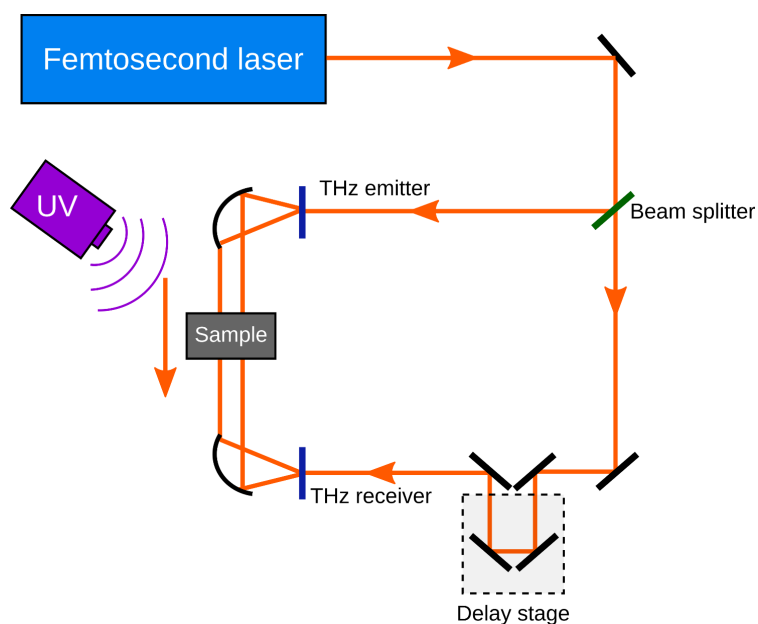


Figure 7. THz Time Domain Spectroscopy test setup.

was aligned until the THz amplitude was at its maximum. Subsequently, the equipment was thermalized for ~1 hour, and the sample was positioned at the focal point of the THz beam path. Five measurements at room temperature were collected for each reference and samples, each of which corresponded to a thousand-point averaging.

Stand-alone PDMS membranes with and without QDs were tested, as well as MM arrays with QDs on the surface and exposed to UV laser excitation of 400 nm in wavelength to determine the prospective modulation behavior of the arrangement.

The obtained THz time domain waveform signal was processed by applying a Gaussian window to remove reflections after the main THz pulse [26] and, subsequently, a Fast Fourier transform (FFT) was employed to obtain the amplitude and phase information of both the reference as well as the sample under consideration. In both cases, *i.e.*, a stand-alone PDMS membrane and MM array, samples without QDs were employed as a reference. The transmittance as a function of frequency of the samples was calculated using the following equation [26]

$$\tilde{T}(\omega) = \frac{\tilde{E}_{sam}(\omega)}{\tilde{E}_{ref}(\omega)} = \frac{A_{sam}(\omega)}{A_{ref}(\omega)} \cdot e^{i(\phi_{sam}(\omega) - \phi_{ref}(\omega))} \quad (4)$$

where \tilde{E}_{sam} and \tilde{E}_{ref} are the complex electric fields, A_{sam} and A_{ref} are the THz amplitudes and ϕ_{sam} and ϕ_{ref} are the phase angles of the sample and reference, respectively. Depending on the sample transmittance results could show specific features as a function of frequency.

3.1. THz Quantum Dot Characterization

From the collected THz-TDS data, optical properties of interest such as refractive index, permittivity and conductivity can be extracted. The real part $n(\omega)$ and imaginary part $\kappa(\omega)$ of the refractive index can be calculated by using the following equations [26]

$$n(\omega) = 1 + \frac{c(\phi_{sam}(\omega) - \phi_{ref}(\omega))}{\omega d} \quad (5)$$

$$\kappa(\omega) = -\left(\frac{c}{\omega d}\right) \ln\left(\left|\frac{A_{sam}(\omega)}{A_{ref}(\omega)}\right|\right) \quad (6)$$

respectively. Similarly, the permittivity and the index of refraction are related by

$$\tilde{\epsilon}(\omega) = \epsilon'(\omega) + i\epsilon''(\omega) = \left(n(\omega)^2 - \kappa(\omega)^2\right) + i(2n(\omega)\kappa(\omega)) \quad (7)$$

where $\tilde{\epsilon}$ is the complex permittivity, ϵ' is the real part of the permittivity, ϵ'' is the imaginary part of the permittivity. The extracted real effective refractive index of the PDMS + QDs membrane at 1 THz (see **Figure 8**), was of ~1.50 for the smaller QDs synthesized with a pH value of 12 (blue dotted line), and to ~1.85 (green solid line) for the larger QDs synthesized with a pH value of 10. Subsequently, the samples were exposed to UV excitation of 400 nm wavelength (see **Figure 9** and **Figure 10**). The intensity of the UV source was measured using

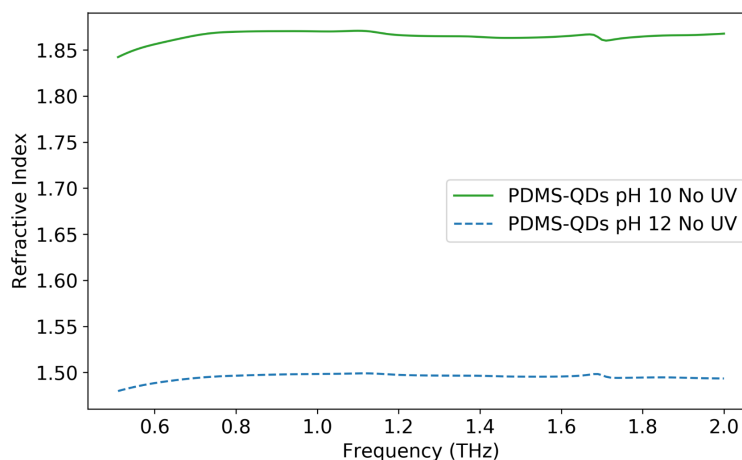


Figure 8. Extracted real part of the effective refractive index of the media with the incorporated ZnO QDs described herein.

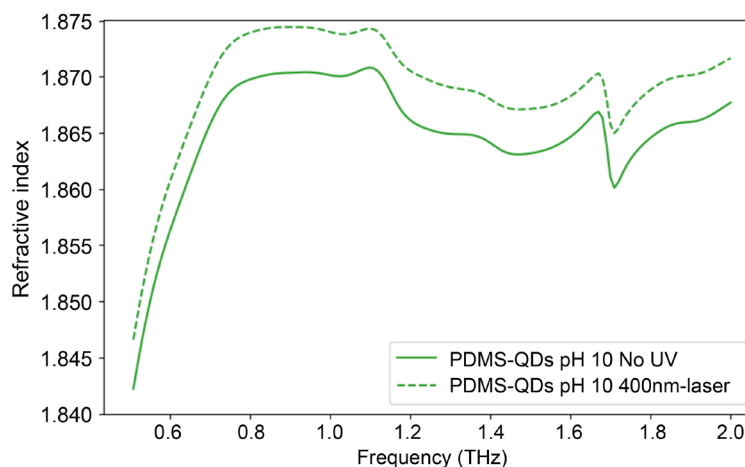


Figure 9. Extracted real part of the refractive index of the medium with the relatively larger ZnO QDs (pH 10) with (dotted line) and without UV excitation of 400 nm (solid line).

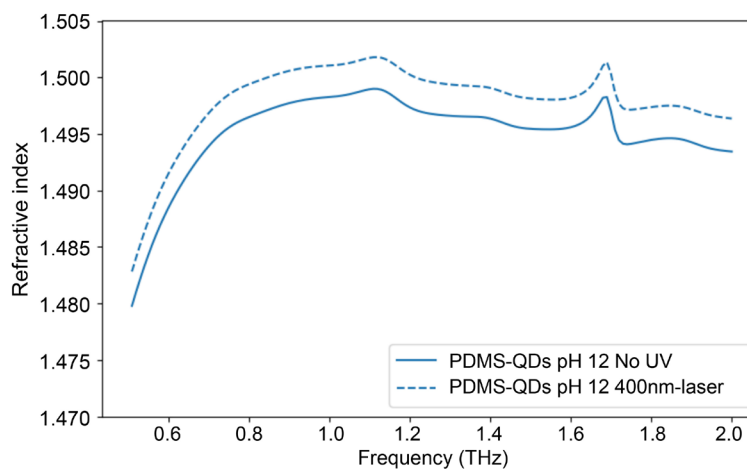


Figure 10. Extracted real part of the refractive index of the medium with the relatively smaller ZnO QDs (pH 12) with (dotted line) and without UV excitation of 400 nm (solid line).

an ILT2400 Light Meter and observed to be 2.5×10^{-4} W/cm². The observations indicate that larger quantum dots exhibit a relatively more pronounced response to UV excitation. This can be explained on the grounds that the synthesized semiconducting nanoparticles exhibit quantum confinement effects where exciton polarizability, reported to be proportional to the fourth power of the radius ($\alpha \sim R^4$), can be defined as [27]

$$\alpha = \frac{\Delta\chi_s (\epsilon_{QD} + 2\epsilon)^2}{9n_s\epsilon^2} \quad (8)$$

were $\Delta\chi_s$ is the susceptibility of the material (related to the permittivity by $\chi_s = 1 - \epsilon$), ϵ_{QD} is the permittivity of the quantum dots, ϵ is the permittivity of the medium and n_s is the sheet excitation density. This result is in agreement with the extracted real part of the effective refractive index of the media with the incorporated ZnO QDs shown in **Figure 8**. Ostensibly, studies of polarizability as a function of frequency and quantum dot dimensions can be performed employing THz-TDS.

3.2. THz Metamaterial Characterization

The experimental characterization of the metamaterial array previously described and shown in **Figure 1**, corroborated the anticipated resonant frequency at 1 THz (dotted lines **Figure 11** and **Figure 12**). Subsequently, the synthesized ZnO QDs were deployed directly on the MM surface, and the resonance frequency was observed to shift to 0.95 THz and to 0.96 THz for the ZnO QDs synthesized with pH values of 10 and 12, respectively. The observed variation in the resonance frequency reflects the permittivity value trends presented in **Figure 8**, thus, larger permittivity values are associated with lower resonant frequencies.

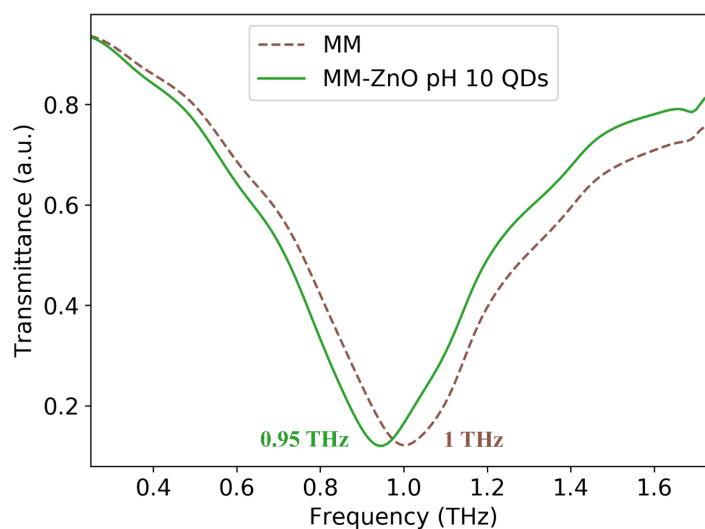


Figure 11. The modification of the effective permittivity of the medium by the deployment of the ZnO QDs synthesized with a pH value of 10, triggered the resonant frequency to decrease from 1 THz to 0.95 THz.

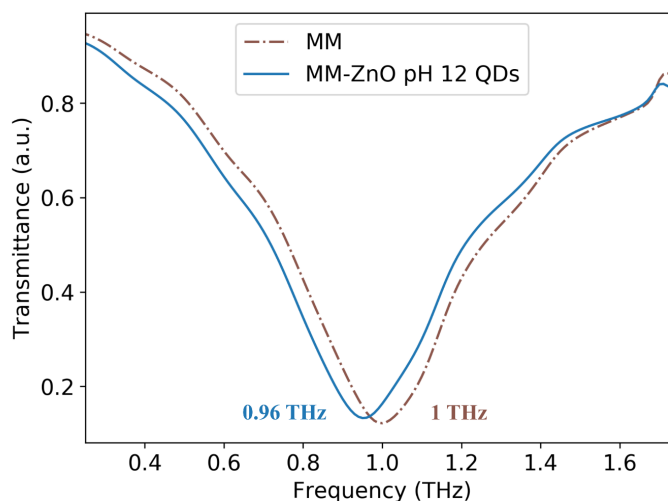


Figure 12. Variation of the resonant frequency of the MM array before (1 THz) and after (0.96 THz) deployment of the ZnO QDs synthesized with a pH value of 12.

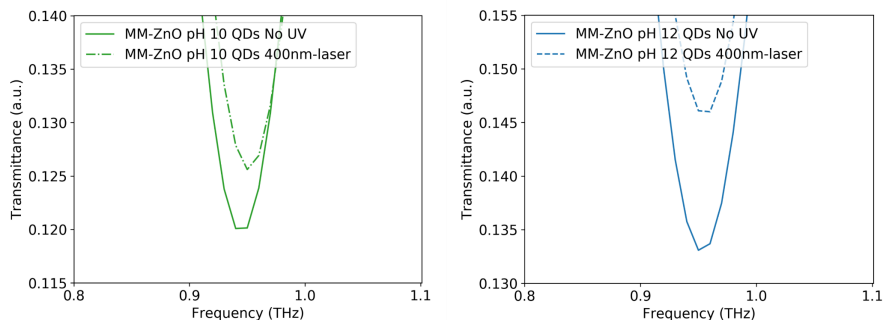


Figure 13. Transmittance calculation of the metamaterial with ZnO pH 10 QDs with and without UV excitation of 400 nm.

In order to measure the modulation of the metamaterial arrays with the deployed quantum dots, the samples were excited with a UV source of 400 nm while being tested with the THz-TDS (results are shown in **Figure 13**). The experimental observations yielded a modulation of 4.55% for the ZnO QDs synthesized with colloidal solutions with a pH value of 10, while the nanoparticles synthesized with a pH value of 12 exhibited a relatively large modulation of 9.21%. The observed results are thought to be due to a higher degree of confinement effects in smaller quantum dots [27]. These changes in modulation depth demonstrate the capability of hexagonal MM via the deployment of ZnO QDs to tune THz electromagnetic signals.

4. Conclusion

ZnO quantum dots were chemically synthesized employing colloidal solutions with pH values of 10 and 12, and the estimated bandgap and radii were calculated to be 3.37 eV (3.00 nm) and 3.50 eV (2.12 nm), respectively. Upon deploying the produced QDs on previously fabricated hexagonal metamaterial arrays and exposing the samples to UV excitation with a wavelength of 400 nm while

performing THz spectroscopy in transmission mode, signal modulation values of 4.55% and 9.21% were observed. The results reported herein could promote the proliferation of THz regime modulation devices. Furthermore, since the photolithographic process for the MM fabrication is mass-production compatible [28], while the ZnO QDs are stable, biologically compatible, and low-cost [29], the MM-ZnO QD setup described herein is considered to be attractive for industrial applications.

Acknowledgements

The authors would like to acknowledge the U.S. Army Research Office (Grant W911NF-13-1-0110), NSF (Grant 1650571) and the Department of Physics and Astronomy at the University of Texas at San Antonio, for the financial support provided for this research project.

Conflicts of Interest

The authors declare no conflicts of interest regarding the publication of this paper.

References

- [1] Hashemi, M.R., Cakmakyapan, S. and Jarrahi, M. (2017) Reconfigurable Metamaterials for Terahertz Wave Manipulation. *Reports on Progress in Physics*, **80**, Article ID: 094501. <https://doi.org/10.1088/1361-6633/aa77cb>
- [2] Davies, A.G., Burnett, A.D., Fan, W., Linfield, E.H. and Cunningham, J.E. (2008) Terahertz spectroscopy of Explosives and Drugs. *Materials Today*, **11**, 18-26. [https://doi.org/10.1016/S1369-7021\(08\)70016-6](https://doi.org/10.1016/S1369-7021(08)70016-6)
- [3] Baaske, K., Salhi, M., Rutz, F., Hasek, T., Wilk, R., Richter, H., *et al.* (2006) Mail Inspection Using THz Imaging: A Comparison of Three Different Systems. *Terahertz for Military and Security Applications IV*, **6212**, 62120U. <https://doi.org/10.1117/12.665238>
- [4] Hernandez-Serrano, A.I., Corzo-Garcia, S.C., Garcia-Sanchez, E., Alfaro, M. and Castro-Camus, E. (2014) Quality Control of Leather by Terahertz Time-Domain Spectroscopy. *Applied Optics*, **53**, 7872-7876. <https://doi.org/10.1364/AO.53.007872>
- [5] Gowen, A.A., O'Sullivan, C. and O'Donnell, C.P. (2012) Terahertz Time Domain Spectroscopy and Imaging: Emerging Techniques for Food Process Monitoring and Quality Control. *Trends in Food Science & Technology*, **25**, 40-46. <https://doi.org/10.1016/j.tifs.2011.12.006>
- [6] Russe, I.S., Brock, D., Knop, K., Kleinebudde, P. and Zeitler, J.A. (2012) Validation of Terahertz Coating Thickness Measurements Using X-Ray Microtomography. *Molecular Pharmaceutics*, **9**, 3551-3559. <https://doi.org/10.1021/mp300383y>
- [7] Ho, L., Müller, R., Römer, M., Gordon, K.C., Heinämäki, J., Kleinebudde, P., *et al.* (2007) Analysis of Sustained-Release Tablet Film Coats Using Terahertz Pulsed Imaging. *Journal of Controlled Release*, **119**, 253-261. <https://doi.org/10.1016/j.jconrel.2007.03.011>
- [8] Woodward, R.M., Cole, B.E., Wallace, V.P., Pye, R.J., Arnone, D.D., Linfield, E.H., *et al.* (2002) Terahertz Pulse Imaging in Reflection Geometry of Human Skin Can-

- cer and Skin Tissue. *Physics in Medicine and Biology*, **47**, 3853-3863. <https://doi.org/10.1088/0031-9155/47/21/325>
- [9] Park, S.J. and Ahn, Y.H. (2015) Terahertz Metamaterials Application in Sensing Bacteria and Fungi. 2015 40th *International Conference on Infrared, Millimeter, and Terahertz Waves (IRMMW-THz)*, Hong Kong, 23-28 August 2015, 1. <https://doi.org/10.1109/IRMMW-THz.2015.7327619>
- [10] Sim, Y.C., Park, J.Y., Ahn, K.-M., Park, C. and Son, J.-H. (2013) Terahertz Imaging of Excised Oral Cancer at Frozen Temperature. *Biomedical Optics Express*, **4**, 1413-1421. <https://doi.org/10.1364/BOE.4.001413>
- [11] Tao, H., Padilla, W.J., Zhang, X. and Averitt, R.D. (2011) Recent Progress in Electromagnetic Metamaterial Devices for Terahertz Applications. *IEEE Journal on Selected Topics in Quantum Electronics*, **17**, 92-101. <https://doi.org/10.1109/JSTQE.2010.2047847>
- [12] Chen, H.T. (2014) Semiconductor Activated Terahertz Metamaterials. *Frontiers of Optoelectronics*, **8**, 27-43. <https://doi.org/10.1007/s12200-014-0436-0>
- [13] Bingham, C.M., Tao, H., Liu, X., Averitt, R.D., Zhang, X. and Padilla, W.J. (2008) Planar Wallpaper Group Metamaterials for Novel Terahertz Applications. *Optics Express*, **16**, 18565-18575. <https://doi.org/10.1364/OE.16.018565>
- [14] Suslick, K.S. and Price, G.J. (1999) Applications of Ultrasound to Materials Chemistry. *Annual Review of Material Science*, **29**, 295-326. <https://doi.org/10.1146/annurev.matsci.29.1.295>
- [15] Pandit, A.B. and Badnore, A.U. (2017) Effect of pH on Sonication Assisted Synthesis of ZnO Nanostructures: Process Details. *Chemical Engineering and Processing: Process Intensification*, **122**, 235-244. <https://doi.org/10.1016/j.cep.2017.09.013>
- [16] Zazueta-Raynaud, A., Pelayo-Ceja, J.E., Lopez-Delgado, R. and Ayon, A. (2016) ZnO Photoluminescent Quantum Dots with Down-Shifting Effect Applied in Solar Cells. *Journal of Physics: Conference Series*, **773**, Article ID: 012036. <https://doi.org/10.1088/1742-6596/773/1/012036>
- [17] Caballero, A.C., Villegas, M., Moure, C. and Ferna, J.F. (2001) Controlled Precipitation Methods: Formation Mechanism of ZnO Nanoparticles. *Journal of the European Ceramic Society*, **21**, 925-930. [https://doi.org/10.1016/S0955-2219\(00\)00283-1](https://doi.org/10.1016/S0955-2219(00)00283-1)
- [18] Alias, S.S., Ismail, A.B. and Mohamad, A.A. (2010) Effect of pH on ZnO Nanoparticle Properties Synthesized by Sol-Gel Centrifugation. *Journal of Alloys and Compounds*, **499**, 231-237. <https://doi.org/10.1016/j.jallcom.2010.03.174>
- [19] Podzorov, A. and Gallot, G. (2010) Density of States and Vibrational Modes of PDMS Studied by Terahertz Time-Domain Spectroscopy. *Chemical Physics Letters*, **495**, 46-49. <https://doi.org/10.1016/j.cplett.2010.06.050>
- [20] Alfihed, S., Bergen, M.H., Holzman, J.F. and Foulds, I.G. (2018) A Detailed Investigation on the Terahertz Absorption Characteristics of Polydimethylsiloxane (PDMS). *Polymer*, **153**, 325-330. <https://doi.org/10.1016/j.polymer.2018.08.025>
- [21] Guzelian, A.A., Katari, J.E.B., Kadavanich, A. V., Banin, U., Hamad, K., Juban, E., *et al.* (1996) Synthesis of Size-Selected, Surface-Passivated InP Nanocrystals. *The Journal of Physical Chemistry*, **100**, 7212-7219. <https://doi.org/10.1021/jp953719f>
- [22] Lin, K.F., Cheng, H.M., Hsu, H.C. and Hsieh, W.F. (2006) Bandgap Engineering and Spatial Confinement of Optical Phonon in ZnO Quantum Dots. 19th *Annual Meeting of the IEEE Lasers and Electro-Optics Society*, Montreal, 29 October-2 November 2006, 939-940. <https://doi.org/10.1109/LEOS.2006.279156>
- [23] Kar, S. and Chaudhuri, S. (2005) Synthesis and Optical Properties of Single and Bi-

crystalline ZnS Nanoribbons. *Chemical Physics Letters*, **414**, 40-46.

<https://doi.org/10.1016/j.cplett.2005.08.021>

- [24] Brus, L. (1986) Electronic Wave Functions in Semiconductor Clusters: Experiment and Theory. *The Journal of Physical Chemistry*, **90**, 2555-2560. <https://doi.org/10.1021/j100403a003>
- [25] MenloSystems (2001) TeraSmart.
- [26] Withayachumnankul, W. and Naftaly, M. (2014) Fundamentals of Measurement in Terahertz Time-Domain Spectroscopy. *Journal of Infrared, Millimeter, and Terahertz Waves*, **35**, 610-637. <https://doi.org/10.1007/s10762-013-0042-z>
- [27] Wang, F., Shan, J., Islam, M.A., Herman, I.P., Bonn, M. and Heinz, T.F. (2006) Exciton Polarizability in Semiconductor Nanocrystals. *Nature Materials*, **5**, 861-864. <https://doi.org/10.1038/nmat1739>
- [28] Zhao, X., Duan, G., Li, A., Chen, C. and Zhang, X. (2019) Integrating Microsystems with Metamaterials towards Metadevices. *Microsystems and Nanoengineering*, **5**, 1-17. <https://doi.org/10.1038/s41378-018-0042-1>
- [29] Patra, M.K., Manoth, M., Singh, V.K., Siddaramana Gowd, G., Choudhry, V.S., Vadera, S.R., *et al.* (2009) Synthesis of Stable Dispersion of ZnO Quantum Dots in Aqueous Medium Showing Visible Emission from Bluish Green to Yellow. *Journal of Luminescence*, **129**, 320-324. <https://doi.org/10.1016/j.jlumin.2008.10.014>